Quantum number fluctuations in the MPD-NICA experiment

MPD Technical note 1

Rodrigo García Formentí and Eleazar Cuautle
Instituto de Ciencias Nucleares, Universidad Nacional Autónoma de México.
Apartado Postal 70-543, Ciudad de México 04510, México

This document presents the methodology for analyzing conserved quantum number fluctuations in the MPD-NICA experiment. The study aims to provide insights into the event-by-event variations of conserved quantities, such as strangeness, which is relevant to locating the critical point of the QCD phase diagram. We used UrQMD data generated and reconstructed in the MPD-NICA for the analysis. We applied efficiency and centrality bin width corrections to the data

I. INTRODUCTION

Understanding the behavior of matter under extreme conditions is a fundamental aspect of Quantum Chromodynamics (QCD). High energy heavy-ion collisions provide an opportunity to study the QCD phase diagram. QCD offers a well-established framework for describing the strong interaction; however, studying its properties at nonzero baryonic chemical potential remains a significant challenge. The properties of QCD matter in the high-baryon density domain have become a very active field of research, particularly in relation to the study of the QCD phase diagram. The existence of a critical end point in the QCD phase diagram is hypothesized and actively investigated on the QCD phase diagram [1, 2], and is a major focus of ongoing heavy-ion collision experiments. The cumulants of conserved quantum numbers, such as electric charge, baryon number, or strangeness, have been shown to be sensitive indicators of critical behavior. The MPD-NICA [3] experiment, currently under development, is designed to explore the QCD phase diagram by studying heavy-ion collisions in the energy range $\sqrt{S_{NN}} = 4$–11 GeV. This energy range is excellent for investigating the critical end point through fluctuations of conserved quantum numbers, which are expected to exhibit abrupt changes in their behavior.
The present document addresses the analysis of cumulants and its corrections for detection efficiency and volume fluctuations.

A. Statistical cumulants

Let ΔN represent the net particle number for a given species (kaons for strangeness, protons for baryon number) within a single event, defined as $\Delta N = N - \bar{N}$ where N is the particle multiplicity and $\bar{N}$ the antiparticle multiplicity per event. Utilizing the average net multiplicity, $\langle \Delta N \rangle$, and the deviation from its mean value, $\delta N = \Delta N - \langle \Delta N \rangle$, the first four cumulants ($C_n,\ n = 1, 2, 3, 4$) are defined as follows:

$$C_1 = \langle \Delta N \rangle, \quad C_2 = \langle (\delta N)^2 \rangle$$

$$C_3 = \langle (\delta N)^3 \rangle, \quad C_4 = \langle (\delta N)^4 \rangle - 3\langle (\delta N)^2 \rangle^2.$$

These cumulants are related to statistical moments as:

$$M = C_1, \quad \sigma^2 = C_2, \quad S = \frac{C_3}{(C_2)^{3/2}}, \quad \kappa = \frac{C_4}{(C_2)^2}. \quad (1)$$

where the parameters of the distribution are: mean (M), standard deviation (σ), skewness (S) and kurtosis (k). In the grand canonical ensemble, the partition function $Z(V, T, \mu)$ governs the statistical behavior of the system. The cumulants of conserved quantities can be expressed in terms of derivatives of $\log Z$ concerning the chemical potential, leading to a direct relation with generalized susceptibilities ($\chi_q^{(n)}$) [4], as

$$C_n = \frac{1}{VT^3} \frac{\partial^n \log Z}{\partial(\mu_q/T)^n} = VT^3 \chi_q^{(n)} \quad (2)$$

where V is the volume, T is the temperature, and μ_q is the chemical potential associated with the conserved number q. The susceptibility can be computed within QCD, directly connecting experimental measurements and theoretical predictions. Moreover, these observables are directly linked to the correlation length and thermodynamic susceptibilities [5]. Critical points are characterized by the divergence of the correlation length (ξ). By utilizing QCD models, we establish a significant link between fluctuation cumulants and the correlation length 3.

$$C_2 \sim \xi^2, \quad C_3 \sim \xi^{4.5}, \quad C_4 \sim \xi^7. \quad (3)$$

To remove explicit volume dependence, we use the following cumulant ratios:

$$\frac{C_1}{C_2} = \frac{M}{\sigma^2}, \quad \frac{C_3}{C_2} = S\sigma, \quad \frac{C_4}{C_2} = \kappa\sigma^2. \quad (4)$$

Given their sensitivity to the correlation length and their connection to susceptibilities, the moments of distributions tied to conserved quantities are sensitive probes for investigating the QCD critical point and the associated phase transition.

II. METHODOLOGY

The analysis was done with two wagons developed within the MpdRoot software framework (version 23.12.24) [6]. The first wagon (Efficiency wagon) provides the detector efficiency calculation while the second wagon (Cumulants wagon) calculates the corrected cumulants with the Factorial Cumulants method [7], using the efficiency output of the first one. Both wagons use the Centrality wagon and the Particle Identification (PID) wagon to compute the first four cumulants of the net-kaon multiplicity distribution across various centrality classes. The wagons have a parameter list:

- mZvtxCut: z vertex cut (cm).
- nPIDsigTPC: maximum $n\sigma$ cut for the TPC.
- nPIDsigTOF: maximum $n\sigma$ cut for the TOF.
- mNofHitsCut: minimal number of TPC hits.
- mEtaCut: maximal pseudorapidity.
- mPtminCut: minimal p_T.
- mPtmaxCut: maximal p_T.
- mDCACut; maximum DCA in therms of $n\sigma$.
- mYCut: maximum rapidity.
- mCentBins: number of bins for the Centrality Bin Width Correction (CBWC).

The analysis is performed for both Monte Carlo generation and reconstructed and identified particles. In the case of reconstructed data, a correction is implemented using factorial moments and identification efficiency. The reconstructed analysis does not depend on Monte Carlo data. The output of the Efficiency wagon is a root file containing the efficiency of charged pions, protons, antiprotons, and charged kaons for all selected centrality bins. The output of the Cumulants wagon is a root file with the factorial moments calculated in the analysis. The cumulants are then computed using factorial moments and efficiency.

A. Analyzed data sample

For this study, the Request 25 [8] dataset provided by the MPD collaboration was used. The dataset consists of Bi+Bi events from the UrQMD event generator collisions at a center-of-mass energy of $\sqrt{s_{NN}} = 9.2$ GeV. A total of 3×10^6 events were analyzed. The Time Projection Chamber (TPC) and the Time-of-Flight (TOF) detectors were used to analyze data.

B. Event Selection

For the events, the following selection criteria were applied:

- Collision vertex z-position: $|V_z| \leq 80$ cm to reject background events which involve interactions with the detectors.
- Presence of at least one charged kaon in the event.

The vertex distribution can be seen in Fig. 1 After cuts,

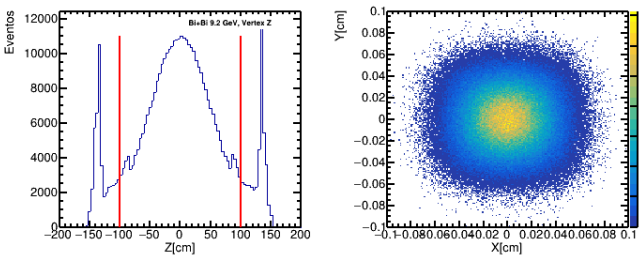

FIG. 1. z-Vertex distribution(left) and $xy-$vertex distribution (right). The region between red lines indicate the events for this analysis.

the data sample was reduced by 50%.

C. Track Selection

For track selection, the following requirements were imposed:

- Minimum number of TPC hits required for track reconstruction: $N_{\text{hits}} \geq 15$ out of a maximum of 54 possible hits in the TPC.
- Distance of closest approach: $|\sigma_{DCA}| \leq 2$ in order to suppress contamination by tracks from secondary vertices.
- Transverse momentum: $0.4 \leq p_T \leq 1.2$ GeV/c.
- Pseudorapidity: $|\eta| \leq 0.5$.

The TPC hits requirement ($N_{hits} > 15$) ensures the quality of the reconstructed tracks, the distribution is shown in Fig. 2

These selection criteria are consistent across the centrality and PID wagons to fully utilize the MPD detector capabilities while ensuring reliable event reconstruction and purity of particle identification.

D. Kaon Identification

Particle identification in the MPD experiment relies on the Time Projection Chamber (TPC) and the Time-of-Flight (TOF) detectors. The TPC records ionization

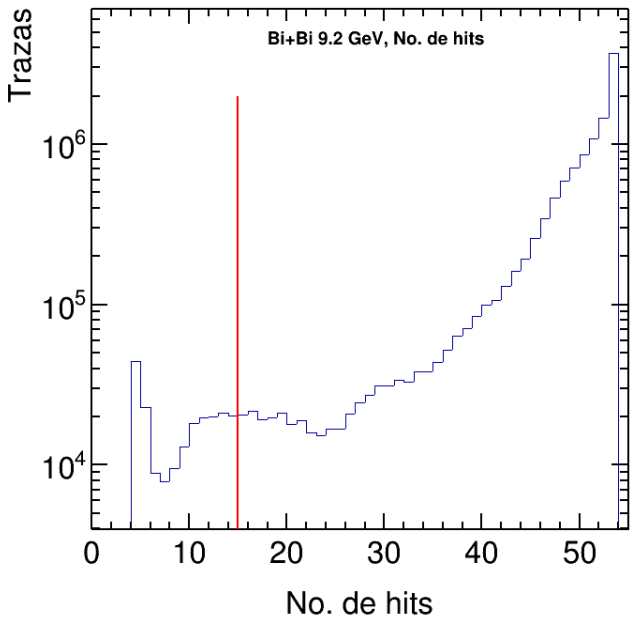

FIG. 2. Number of TPC hits distribution. The red lines represent the lower limits for this analysis.

signals as particles traverse the detector, providing measurements of energy loss. The TOF detector measures the time of flight of particles, allowing mass determination. Combining information from both detectors enhances the accuracy of particle identification. To ensure correct TOF matching with TPC, and prevent track mismatches, a selection of the number of sigmas on z coordinate in the TOF ($n\sigma\text{TOF}dz$) and the number of sigmas on azimuthal angle, ϕ, on TOF ($n\sigma\text{TOF}d\phi$), are shown in Fig. 3. The tracks satisfying cuts of $|n\sigma\text{TOF}dz| < 2$ and $|n\sigma\text{TOF}d\phi| < 2$ indicated by horizontal lines, are considered good for the analysis.

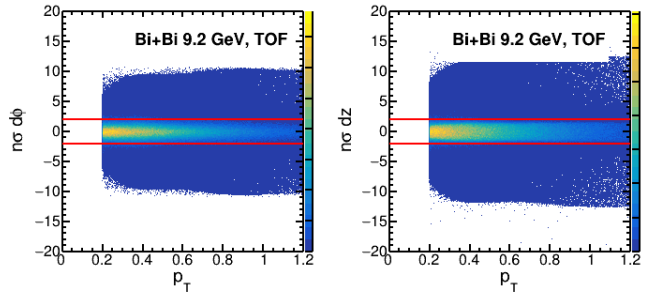

FIG. 3. $n\sigma\text{TOF}dz$ (left) and $n\sigma\text{TOF}d\phi$ (right) distributions. The selected tracks are between the red lines.

To ensure maximum efficiency in the identification, momentum-dependent selection criteria are employed: The TOF information is used for tracks with $p_T \geq 0.5$ GeV. This selection criterion was applied after analyzing the TOF efficiency, defined as

$$\epsilon_{\text{TOF}}(p_T) = \frac{N_{\text{TOF}}(p_T)}{N_{\text{TPC}}(p_T)} \tag{5}$$

where N_{TPC} is the number of tracks registered using the TPC and N_{TOF} is the number of tracks registered using TOF. The TOF efficiency is shown in Fig. 4. For tracks with $p_T \leq 0.5$ GeV/c, if there is a mismatch ($|n\sigma\text{TOF}dz| > 2$ or $|n\sigma\text{TOF}d\phi| > 2$), only TPC information is used. For all other cases ($p_T > 0.5$), both TPC and TOF information are used to maximize identification accuracy.

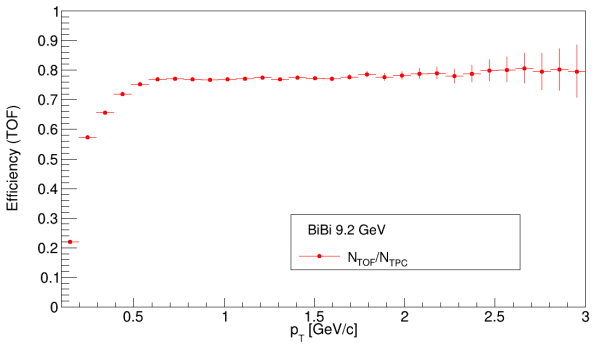

FIG. 4. TOF efficiency.

The list of selection criteria applied for kaon identification is as follows:

- $p_T \leq 0.5$ GeV/c, if $|n\sigma\text{TOF}dz| > 2$ or $|n\sigma\text{TOF}d\phi| > 2$, then the identification criteria is $|n\sigma\text{TPC}(K)| < 2$ and (TPC-only identification).
- $p_T \leq 0.5$ GeV/c, if $|n\sigma\text{TOF}dz| < 2$ or $|n\sigma\text{TOF}d\phi| < 2$, the identification criteria is $|n\sigma\text{TPC}(K)| < 2$, and $|n\sigma\text{TPC}(K)| < 2$ (TPC+TOF identification).
- $p_T > 0.5$ GeV/c, the identification criteria is $|n\sigma\text{TPC}(K)| < 2$, $|n\sigma\text{TOF}dz| < 2$, $|n\sigma\text{TOF}d\phi| < 2$, $|n\sigma\text{TPC}(K)| < 2$ (TPC+TOF identification)

Distributions of the number of sigmas on TPC ($n\sigma\text{TPC}^K$) and TOF ($n\sigma\text{TOF}^K$) are presented in Fig. 5, where the selected tracks are those between horizontal lines.

The distributions of the average energy loss and square mass, respectively, as a function of the transverse momentum normalized to the charge, are shown before cuts in Fig. 6, and after cuts in Fig. 7.

The efficiency of the kaon identification as a function of transverse momentum is defined as

$$\epsilon_{\text{PID}}^{K^\pm} = \frac{\text{Num. of K identified}}{\text{Num. of K generated}} \tag{6}$$

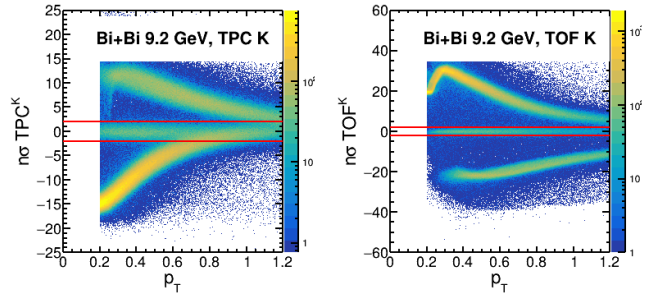

FIG. 5. $n\sigma\text{TPC}(K)$ (left) and $n\sigma\text{TOF}(K)$ (right) distributions as a funciton of transverse momentum. The selected traces are between the red lines.

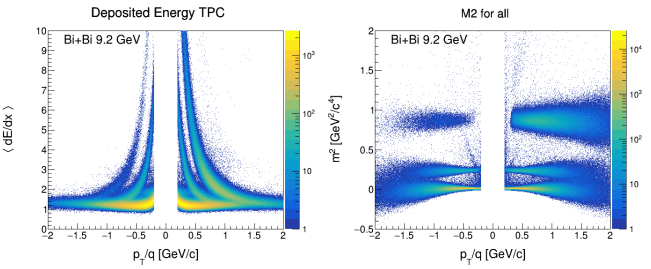

FIG. 6. Energy deposited in TPC (left) and the m^2 in TOF (right) distributions as a function of transverse momentum normalized before particle identification.

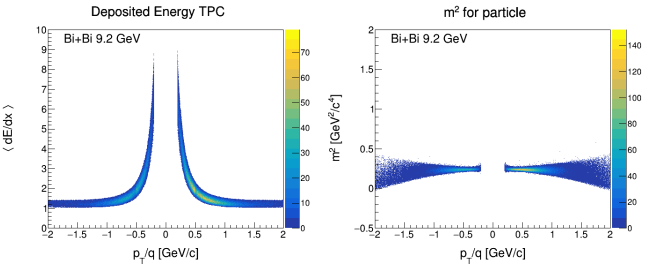

FIG. 7. Energy deposited in TPC (left) and the m^2 in TOF (right) distributions as a function of transverse momentum normalized after kaon identification.

while the purity and the contamination are defined as

$$\text{pur}_{\text{PID}}^{K^\pm} = \frac{\text{Num. of True positive identified } K^\pm}{\text{Num. of } K^\pm \text{ identified}}, \quad (7)$$

$$\text{cont}_{\text{PID}}^{K^\pm} = \frac{\text{Num. of False positive identified } K^\pm}{\text{Num. of } K^\pm \text{ identified}} \quad (8)$$

where the generated K corresponds to Monte Carlo K. The efficiency of particle identification as a function of transverse momentum is displayed in Fig. 8, while Fig. 9 illustrates contamination and purity of the identification process. Purities of K^+ and K^- samples are better than 98% for all the p_T range.

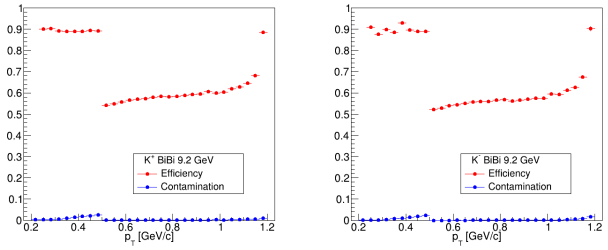

FIG. 8. Efficiency distribution of identification for K^+ (left) and K^- (right)

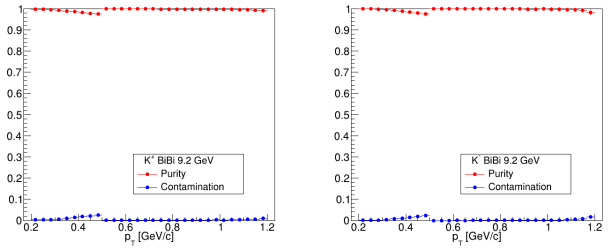

FIG. 9. Purity and contamination of identification for K^+ (left) and K^- (right)

III. RESULTS AND DISCUSSION

A. Uncorrected net kaon multiplicity distributions and Cumulants

In Fig. 10, the net multiplicity of kaons is shown for Monte Carlo data, minimum bias at generation and reconstructed level, for central (0%-10%), and peripheral (50%-60%) collisions. An increase in discrepancy is observed going from peripheral to central collisions.
Fig 11 shows the first four cumulants (C1,C2, C3, C4) and the ratios C3/C2 and C4/C2 for Monte Carlo (with legend MC) and reconstructed (with legend PID) kaons. As expected, these raw values are affected by acceptance and efficiency effects, and don't yet reflect the true physics.

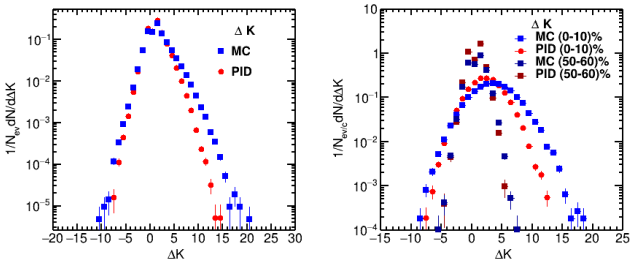

FIG. 10. Net multiplicity of kaons. In blue, Monte Carlo data (MC), in red reconstructed data (PID). Without centrality selection (left), and for central and peripheral collisions (right).

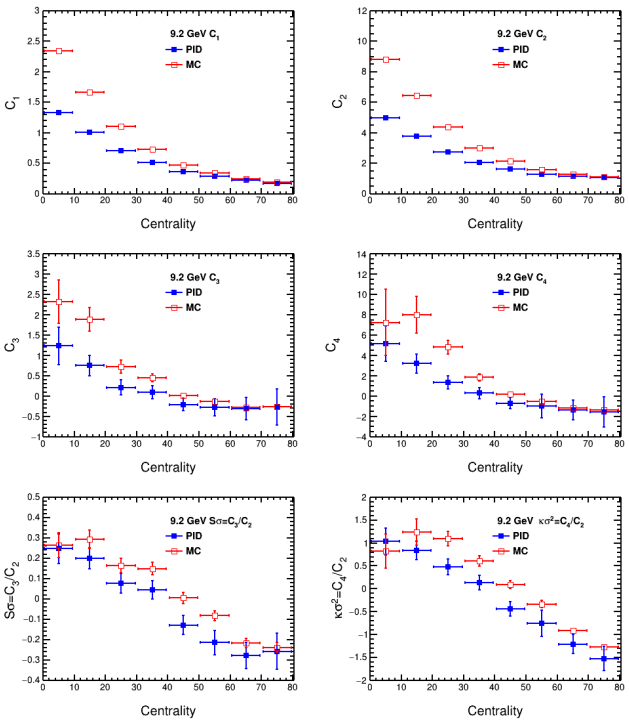

FIG. 11. First four cumulants and cumulant ratios of Kaon net multiplicity distribution as a function of the centrality. In blue, the Monte Carlo data, while in red, the reconstructed data.

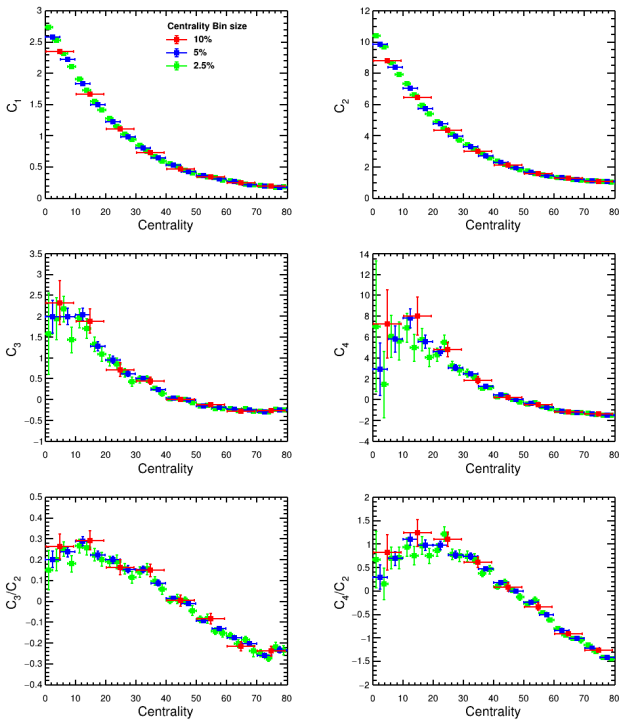

FIG. 12. Cumulants of the net kaon multiplicity as a function of centrality calculated for 10%, 5%, and 2.5% centrality bin width.

.

B. Volume fluctuation correction

The initial collision geometry is estimated using particle multiplicities, which cannot be measured directly. This introduces a centrality bin width effect caused by volume variations [9] within a finite centrality bin size. To mitigate this effect, we employ the Centrality Bin Width Correction (CBWC) [10, 11] where the cumulants are calculated using:

$$C_i = \frac{\sum_r n_r C_{i,r}}{\sum_r n_r}, \tag{9}$$

where n_r represents the number of events in the r-th multiplicity bin for the centrality determination, $C_{i,r}$ are the i-th order cumulants of particle number distributions at r-th multiplicity. The cumulants are sensitive to error; to mitigate the event loss from choosing multiplicity bins, finite centrality bins were used. Fig. 12 shows the calculated cumulants as a function of centrality for different centrality bin sizes (10%, 5% and 2.5%), Fig. 13 shows the cumulant calculation as a function of centrality, corrected by CBWC, for three centrality bin width sizes: 10%, 5% and 2.5%.

For the third and fourth cumulants, it is clear that the 10% centrality bin width exhibits significant deviations compared to those with 5% and 2.5%. This result highlights the importance of considering the CBWC. In Ref.[12], it is shown that 2.5% almost overlaps the cumulants with CBWC.

C. Efficiency correction

Due to finite detection efficiency and its dependence on transverse momentum, it is necessary to implement corrections [13]. Assuming a detector 100% efficiency, the produced net particles (N) follow a probability distribution function, $P(N)$, while the measured particles n follow:

$$p(n) = \sum_N w(n|N)P(N), \tag{10}$$

where $w(n|N)$ denotes the probability distribution of observing n particles given N produced particles. The probability distribution, $w(n|N)$ in Eq. 10 can be modeled using a binomial distribution. The factorial moments (F_{ik}), of the $P(N)$, and f_{ik} for the $p(n)$, distributions are defined as [14]:

$$F_{ik} = \left\langle \frac{N!}{(N-i)!} \frac{\overline{N}}{(\overline{N}-k)!} \right\rangle, \quad f_{ik} = \left\langle \frac{n!}{(n-i)!} \frac{\overline{n}}{(\overline{n}-k)!} \right\rangle \tag{11}$$

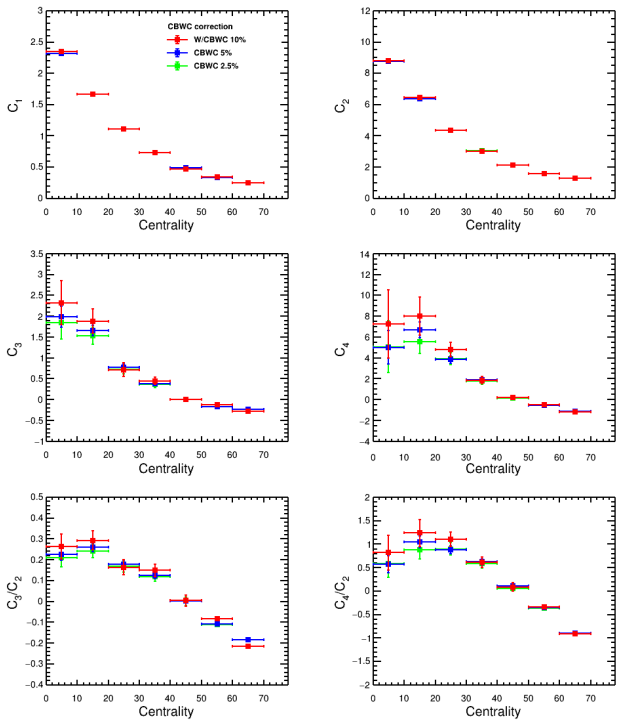

FIG. 13. Cumulants of the net kaon multiplicity as a function of centrality calculated with correction using bin size of 10%, 5%, and 2.5%.

.

where the overline refers to antiparticles. The factorial moments are related to the first four cumulants as:

$$C_1 = F_{01} - F_{02}, \tag{12}$$
$$C_2 = N - C_1^2 + F_{02} - 2F_{11} + F_{20}, \tag{13}$$
$$C_3 = C_1 + 2C_1^3 - F_{03} - 3F_{02} + 3F_{12} + 3F_{20} - 3F_{21} + F_{30} - 3C_1(N + F_{02} - 2F_{11} + F_{20}), \tag{14}$$
$$C_4 = N - 6C_1^4 + F_{04} + 6F_{03} + 7F_{02} - 2F_{11} - 6F_{12} - 4F_{13} + 7F_{20} - 6F_{21} + 6F_{22} + 6F_{30} - 4F_{31} + F_{40} + 12C_1^2(N + F_{02} - 2F_{11} + F_{20}) - 3(N + F_{02} - 2F_{11} + F_{20})^2 - 4C_1(C_1 - F_{03} - 3F_{02} + 3F_{12} + 3F_{20} - 3F_{21} + F_{30}). \tag{15}$$

To incorporate transverse momentum dependence to the efficiency [7, 15] from the particle x, and from the negative particle $\overline{x}$, we introduce local factorial moments A_{ik} and a_{ik}:

$$A_{ik}\,(x_1,\ldots,x_i;\overline{x}_1,\ldots,\overline{x}_i) = \langle N(x_1)[N(x_2)-\delta_{x_1,x_2})]\cdots [N(x_i)-\delta_{x_1,x_i}-\cdots-\delta_{x_{i-1},x_i}]\overline{N}(\overline{x}_2)-\delta_{\overline{x}_1,\overline{x}_2})]\cdots [\overline{N}(\overline{x}_i)-\delta_{x_1,x_i}-\cdots-\delta_{x_{i-1},x_i}]\rangle, \tag{16}$$

$$a_{ik}\,(x_1,\ldots,x_i;\overline{x}_1,\ldots,\overline{x}_i) = \langle n(x_1)[n(x_2)-\delta_{x_1,x_2})]\cdots [n(x_i)-\delta_{x_1,x_i}-\cdots-\delta_{x_{i-1},x_i}]\overline{n}(\overline{x}_2)-\delta_{\overline{x}_1,\overline{x}_2})]\cdots [\overline{n}(\overline{x}_i)-\delta_{x_1,x_i}-\cdots-\delta_{x_{i-1},x_i}]\rangle, \tag{17}$$

were the subscripts refer to the transverse momentum bins used in the correction. Using the relations

$$F_{ik} = \sum_{x_1,\ldots,x_i}\sum_{\overline{x}_1,\ldots,\overline{x}_i} A_{ik}(x_1,\ldots,x_i;\overline{x}_1,\ldots,\overline{x}_i) \tag{18}$$

and

$$a_{ik} = \epsilon(x_1)\ldots\epsilon(x_i)\overline{\epsilon}(\overline{x}_1)\ldots\overline{\epsilon}(\overline{x}_i)A_{ik}, \tag{19}$$

where ϵ and $\overline{\epsilon}$ are the local efficiency of the detector to identify the particle N and $\overline{N}$. Using the equations 18 and 19, we get the relation between the factorial cumulants of the produced particle distribution and the measured local factorial moments Eq. 18

$$F_{ik} = \sum_{x_1,\ldots,x_i}\sum_{\overline{x}_1,\ldots,\overline{x}_i} \frac{a_{ik}(x_1,\ldots,x_i;\overline{x}_1,\ldots,\overline{x}_i)}{\epsilon(x_1)\ldots\epsilon(x_i)\overline{\epsilon}(\overline{x}_1)\ldots\overline{\epsilon}(\overline{x}_i)}. \tag{20}$$

To correct the data, we have to select the bin size in the efficiency distribution. In Fig. 14 an efficiency distribution is shown with four different bins. Using this distribution, the corrected cumulants are shown in Fig. 15.

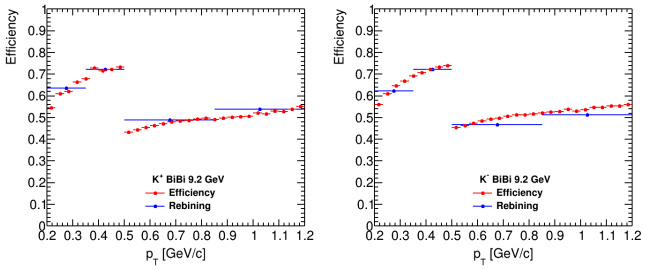

FIG. 14. Efficiency (red) and efficiency rebining used in the correction (blue) for K^+ (left) and K^- (right) identification.

After applying local efficiency corrections, we obtain the cumulants of the net-kaon multiplicity distributions as a function of centrality. As can be seen, the corrected cumulants can now be studied.

IV. STATISTICAL UNCERTAINTY

Since higher-order cumulants are particularly sensitive to the shape of the multiplicity distributions, a precise estimation of statistical uncertainties is essential. In this analysis, the Delta theorem method [14, 16] and Bootstrap method [14, 17] were used.

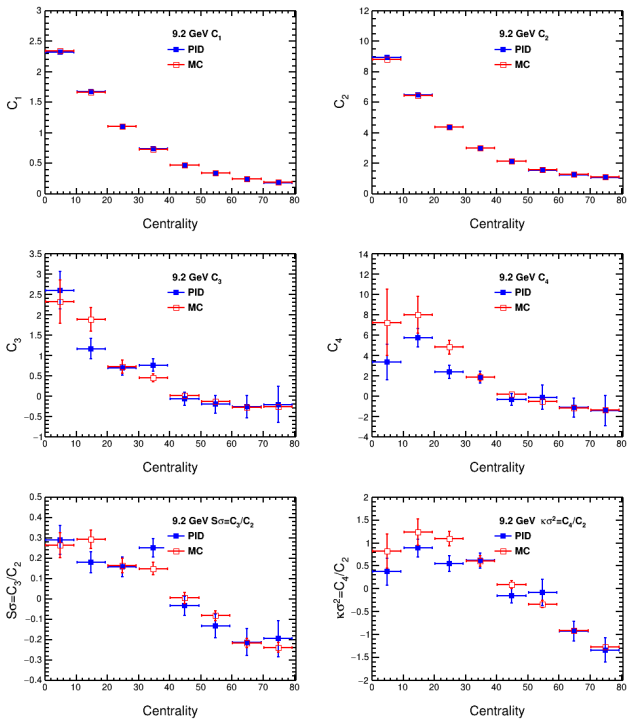

FIG. 15. Cumulants of the net kaon multiplicity as a function of centrality. Using Monte Carlo data (blue) and corrected using efficiency binning.

A. Delta Theorem method

This method uses the central limit theorem, in which the variance of the statistic C_n can be calculated as [12]:

$$V(C_n) = \sum_{i,j=1} \left(\frac{\partial C_n}{\partial X_i}\right)\left(\frac{\partial C_n}{\partial X_j}\right) \mathrm{Cov}(X_i, X_j), \quad (21)$$

where $\mathrm{Cov}(X_i, X_j)$ is the covariance between the random variables X_i and X_j. The efficiency corrected cumulants and moments are expressed in terms of factorial moments. The covariance between factorial moments is [14]

$$\mathrm{Cov}(f_{r,s}, f_{u,v}) = \frac{1}{n}(f_{(ru),(sv)} - f_{rs} f_{uv}), \quad (22)$$

where $f_{(ru),(su)}$ is defined as:

$$f_{(ru),(su)} = \left\langle \frac{X_1!}{(X_1-r)!}\frac{X_1!}{(X_1-u)!}\frac{X_2!}{(X_2-s)!}\frac{X_2!}{(X_1-v)!} \right\rangle . \quad (23)$$

If the acceptance of the kaon is $\epsilon = 1$, the statistical uncertainties can be expressed as the square roots of the variances:

$$\mathrm{Var}(C_1) = \mu_2/n, \quad (24)$$
$$\mathrm{Var}(C_2) = (-\mu_2^2 + \mu_4)/n, \quad (25)$$
$$\mathrm{Var}(C_3) = (9\mu_2^3 - 6\mu_2\mu_4 - \mu_3^2 + \mu_6)/n, \quad (26)$$
$$\mathrm{Var}(C_4) = (-36\mu_2^4 + 48\mu_2^2\mu_4 + 64\mu_2\mu_3^2 \quad (27)$$
$$- 12\mu_2\mu_6 - 8\mu_3\mu_5 - \mu_4^2 + \mu_8)/n. \quad (28)$$

where $\mu_n = \langle(\delta N)^n\rangle$ are the nth-order central moments. This means that statistical uncertainty depends on the width of the distribution. For similar event statistics, the statistical uncertainties are larger in central collisions than in peripheral collisions. To add the efficiency dependence to the statistical uncertainties we used the formula

$$\mathrm{Err}(C_n) \propto \frac{\sqrt{\mathrm{Var}(C_n)}}{\epsilon^\alpha}. \quad (29)$$

where n is an integer, ϵ is the efficiency and $\alpha > 0$ is a real number.

B. Bootstrap method

The Bootstrap method is a computer intensive resampling method [14]. If we have a sample of N events, one makes B new samples with N events, which are chosen randomly with replacement from the original sample. We calculate the quantity C_n with all the B samples, and the uncertainty of the quantity is estimated by the variance of the quantities of the B samples,

$$V(C_n) = \frac{B}{B-1}\left[\frac{1}{B}\sum_{b=1}^{B}(C_n^b)^2 - \left(\frac{1}{B}\sum_{b=1}^{B} C_n^b\right)\right] \quad (30)$$

where C_n^b is the cumulant for the sample number b. In this analysis, we divided the number of events N into 150 sets, each containing 20000 events, to create the new samples, and the total number of new samples is $B = 150$. The bootstrap method has complications if the quantity whose variance is being estimated depends heavily on the tails of the distribution. In Ref.[14, 18], the Bootstrap method is compared with the Delta method, showing that the Bootstrap method can be used to compute the statistical errors.

V. OUTLOOK

A. Centrality self-correlations

Self-correlation effects appear when the centrality classes are calculated using the particles used for fluctuation analyses (in this example, the kaons). To eliminate this effect, it is important to exclude kaons from charged particles for centrality selection [10]. This means it is necessary to redefine centrality and add a new wagon or update the Centrality Wagon to calculate the centrality for the fluctuations analyses.

B. Volume fluctuations correction

The Centrality Bin Width Correction (CBWC) provides an approximation to reduce the dependence on volume fluctuations. This effect can be mitigated by assuming that, for any r-th multiplicity bin, the corresponding average volume V^r is proportional to the mean number of participants $\langle N^r_{\rm part}\rangle$:

$$V^r = \langle N^r_{\rm part}\rangle V_0 \tag{31}$$

where $V_0 = 2.83, \mathrm{fm}^3$ [19]. We then substitute

$$n_r \to N^r = \frac{n_r}{V^r} \tag{32}$$

to compute the cumulants. This yields the reduced deviation

$$\delta N^r = \frac{n_r}{V^r} - \left\langle \frac{n_r}{V^r} \right\rangle \tag{33}$$

for the distribution of the conserved quantity N^r. To apply this correction, only the mean number of participants in each multiplicity bin, $\langle N^r_{\rm part}\rangle$, is required, as suggested in Ref. [20]. This feature can be integrated into the Centrality Wagon in a future update.

C. Another centrliaty definition

A new centrality definition for analyzing higher-order cumulants was proposed in Ref. [21], to reduce volume fluctuations; however, the possible improvement could be done with real data to compare with the correction method described here.

VI. CONCLUSION AND FINAL REMARKS

In this technical note, we present a systematic analysis of the cumulants of strangeness as conserved quantum numbers. The methodology applied considers Monte Carlo data generated with UrQMD and reconstructed with MPDRoot within the MPD. Computed cumulants were corrected by efficiency and centrality bins. The results suggest that in a clean sample of around 10^6 events, the MPD experiment will be able to measure the cumulants. However, the error should be analyzed carefully to obtain a better understanding than what is published. This analysis can be extended for baryon number conservation.

ACKNOWLEDGMENTS

We thank Victor Riabov, for the feedback. R.G.F. acknowledges the financial support of fellowships granted by Secretaría de Ciencia, Humanidades, Tecnología e Innovación (SECIHTI). Partial support was received by DGAPA-PAPIIT IG100826 and CONAHCyT-CF-2023-G-433 projects.

VII. REFERENCES

[1] L. Du, A. Sorensen, and M. Stephanov, The QCD phase diagram and Beam Energy Scan physics: A theory overview, Int. J. Mod. Phys. E **33**, 2430008 (2024), arXiv:2402.10183 [nucl-th].
[2] M. A. Stephanov, QCD phase diagram: An Overview, PoS **LAT2006**, 024 (2006), arXiv:hep-lat/0701002.
[3] V. Abgaryan et al. (MPD), Status and initial physics performance studies of the MPD experiment at NICA, Eur. Phys. J. A **58**, 140 (2022), arXiv:2202.08970 [physics.ins-det].
[4] F. Karsch and K. Redlich, Probing freeze-out conditions in heavy ion collisions with moments of charge fluctuations, Phys. Lett. B **695**, 136 (2011), arXiv:1007.2581 [hep-ph].
[5] M. A. Stephanov, Non-Gaussian fluctuations near the QCD critical point, Phys. Rev. Lett. **102**, 032301 (2009), arXiv:0809.3450 [hep-ph].
[6] M. colaboration, The mpdroot, `https://mpdroot.jinr.ru/`, accessed: (2025).
[7] A. Bzdak and V. Koch, Local Efficiency Corrections to Higher Order Cumulants, Phys. Rev. C **91**, 027901 (2015), arXiv:1312.4574 [nucl-th].
[8] M. colaboration, Request 25: General-purpose, 50m urqmd bibi@9.2, `https://mpdforum.jinr.ru/\t/request-25-general-purpose-50m-urqmd-bibi-9-2\-second-collaboration-paper/455` (2022), accessed: (2025).
[9] A. Chatterjee, Y. Zhang, J. Zeng, N. R. Sahoo, and X. Luo, Effect of centrality selection on higher-order cumulants of net-proton multiplicity distributions in relativistic heavy-ion collisions, Phys. Rev. C **101**, 034902 (2020), arXiv:1910.08004 [nucl-ex].
[10] X. Luo, J. Xu, B. Mohanty, and N. Xu, Volume fluctuation and auto-correlation effects in the moment analysis of net-proton multiplicity distributions in heavy-ion collisions, J. Phys. G **40**, 105104 (2013), arXiv:1302.2332 [nucl-ex].
[11] P. Braun-Munzinger, A. Rustamov, and J. Stachel, Bridging the gap between event-by-event fluctuation measurements and theory predictions in relativistic nuclear collisions, Nucl. Phys. A **960**, 114 (2017), arXiv:1612.00702 [nucl-th].
[12] M. Abdallah et al. (STAR), Cumulants and correlation functions of net-proton, proton, and antiproton multiplicity distributions in Au+Au collisions at energies available at the BNL Relativistic Heavy Ion Collider, Phys. Rev. C **104**, 024902 (2021), [Erratum: Phys.Rev.C 111, 029902 (2025)], arXiv:2101.12413 [nucl-ex].
[13] A. Bzdak and V. Koch, Acceptance corrections to net baryon and net charge cumulants, Phys. Rev. C **86**, 044904 (2012), arXiv:1206.4286 [nucl-th].

[14] X. Luo, Unified description of efficiency correction and error estimation for moments of conserved quantities in heavy-ion collisions, Phys. Rev. C **91**, 034907 (2015), [Erratum: Phys.Rev.C 94, 059901 (2016)], arXiv:1410.3914 [physics.data-an].

[15] F. Si and Y. Zhang, Statistical uncertainty estimation of higher-order cumulants with finite efficiency and its application in heavy-ion collisions, Phys. Rev. C **105**, 024907 (2022), arXiv:2111.00238 [nucl-th].

[16] X. Luo, Error Estimation for Moments Analysis in Heavy Ion Collision Experiment, J. Phys. G **39**, 025008 (2012), arXiv:1109.0593 [physics.data-an].

[17] B. Efron, Bootstrap methods: Another look at the jackknife, The Annals of Statistics 7 p1-26 (1979).

[18] A. Pandav, D. Mallick, and B. Mohanty, Effect of limited statistics on higher order cumulants measurement in heavy-ion collision experiments, Nucl. Phys. A **991**, 121608 (2019), arXiv:1809.08892 [nucl-ex].

[19] V. Skokov, B. Friman, and K. Redlich, Volume fluctuations and higher-order cumulants of the net baryon number, Physical Review C **88**, 10.1103/physrevc.88.034911 (2013).

[20] G. Feofilov, Proton and net-proton high-order cumulants: can we do better with mpd at nica?, `https://indico.jinr.ru/event/5294/` (2025), accessed: (2025).

[21] Z. Wang and X. Luo, A Centrality-independent Framework for Revealing Genuine Higher-Order Cumulants in Heavy-Ion Collisions, (2025), arXiv:2505.03666 [physics.data-an].